International Scholarly Research Network
ISRN Nanotechnology
Volume 2012, Article ID 539601, 8 pages
doi:10.5402/2012/539601

Review Article

Dissolvable Trimolybdate Nanowires as Ag Carriers for High-Efficiency Antimicrobial Applications

Jiongwei Xue,[1] Jianwen Ye,[1] Yujie Jiang,[1] Mo Chen,[1] Huayong Pan,[1] Shengyong Xu,[1] Wei Wang,[2] and Jie Tang[2]

[1] *Key Laboratory for the Physics and Chemistry of Nanodevices and School of Electronics Engineering and Computer Science, Peking University, Beijing 100871, China*
[2] *Institute of Biophysics, Chinese Academy of Sciences, 15 Datun Road, Chaoyang District, Beijing 100101, China*

Correspondence should be addressed to Shengyong Xu, xusy@pku.edu.cn and Jie Tang, jtang@ibphys.cas.cn

Received 5 October 2011; Accepted 9 November 2011

Academic Editors: C. A. Charitidis and C. Malagù

Elimination of bacteria and other microbes effectively is important to our daily life and a variety of medical applications. Here, we introduce a new kind of trimolybdate nanowires, namely $Ag_{2-x}(NH_4)_xMo_3O_{10} \cdot 3H_2O$, that carry a large amount of Ag atoms in the lattice and Ag-rich nanoparticles on the surface. These nanowires can eliminate bacteria of *E. coli*, *Staphylococcus aureus*, and unknown microbes in raw natural water with high efficiency. For example, they can inactivate more than 98% of *E. coli* with a nanowire concentration of only 5 ppm in the solution. The excellent sterilization performance is attributed to the combined effects of Ag ions, Mo ions, and Ag-rich nanoparticles of the $Ag_{2-x}(NH_4)_xMo_3O_{10} \cdot 3H_2O$ nanowires. These nanowires are not dissolvable in deionized water but can be dissolved by the metabolic materials released from bacteria, making them attractive for many biological applications.

1. Introduction

Silver (Ag), in the form of bulk, sheet, wire, powder, and composite, has a long history of being used as a broad-spectrum antimicrobial material [1–7]. In particular, with a high surface-to-volume ratio, Ag nanoparticles showed much higher antimicrobial efficiency than Ag microparticles [8–16]. In some biological applications, it should be rather interesting if Ag composites or nanoparticles could be delivered to target tissues and/or cells with a controllable carrier of nanomaterial. Similar concepts have already been well presented in studies on drug delivery of molecular medicines, characterization, imaging, and targeting with carbon nanotubes, nanowires, and other nanomaterials [16–28]. However, in these approaches, side effects caused by the residual nanomaterials inside tissues or cells become a great concern. Some nanomaterials, such as carbon nanotubes, are chemically and biologically inert, and *in vivo* studies showed that they could accumulate and be permanently trapped in living organs or tissues, causing unexpected multiple toxicity [29–33].

Here, we introduce a new kind of trimolybdate nanowires, namely $Ag_{2-x}(NH_4)_xMo_3O_{10} \cdot 3H_2O$, that carry a large amount of Ag atoms in the lattice and Ag-rich nanoparticles on the surface. Similar to previously reported powders of Ag_2MoO_4, $Ag_2Mo_2O_7$, $Ag_6Mo_{10}O_{33}$, $Ag_2Mo_3O_{10} \cdot 1.8H_2O$, and so forth [34–37], the $Ag_{2-x}(NH_4)_xMo_3O_{10} \cdot 3H_2O$ nanowires show strong antimicrobial properties, for example, they kill *E. coli*, *Staphylococcus aureus,* and unknown microbes in raw natural water with high efficiency. The nanowires are not dissolvable in deionized water; however they could be dissolved by the metabolic chemicals released from bacteria, making them attractive for many biological applications.

2. Materials and Methods

The $Ag_{2-x}(NH_4)_xMo_3O_{10} \cdot 3H_2O$ nanowires and other nanomaterials were synthesized from a mixed aqueous solution of $(NH_4)_6Mo_7O_{24} \cdot 4H_2O$ (purity 99.999%) and $AgNO_3$ (purity 99.999%) that were separately dissolved in deionized water.

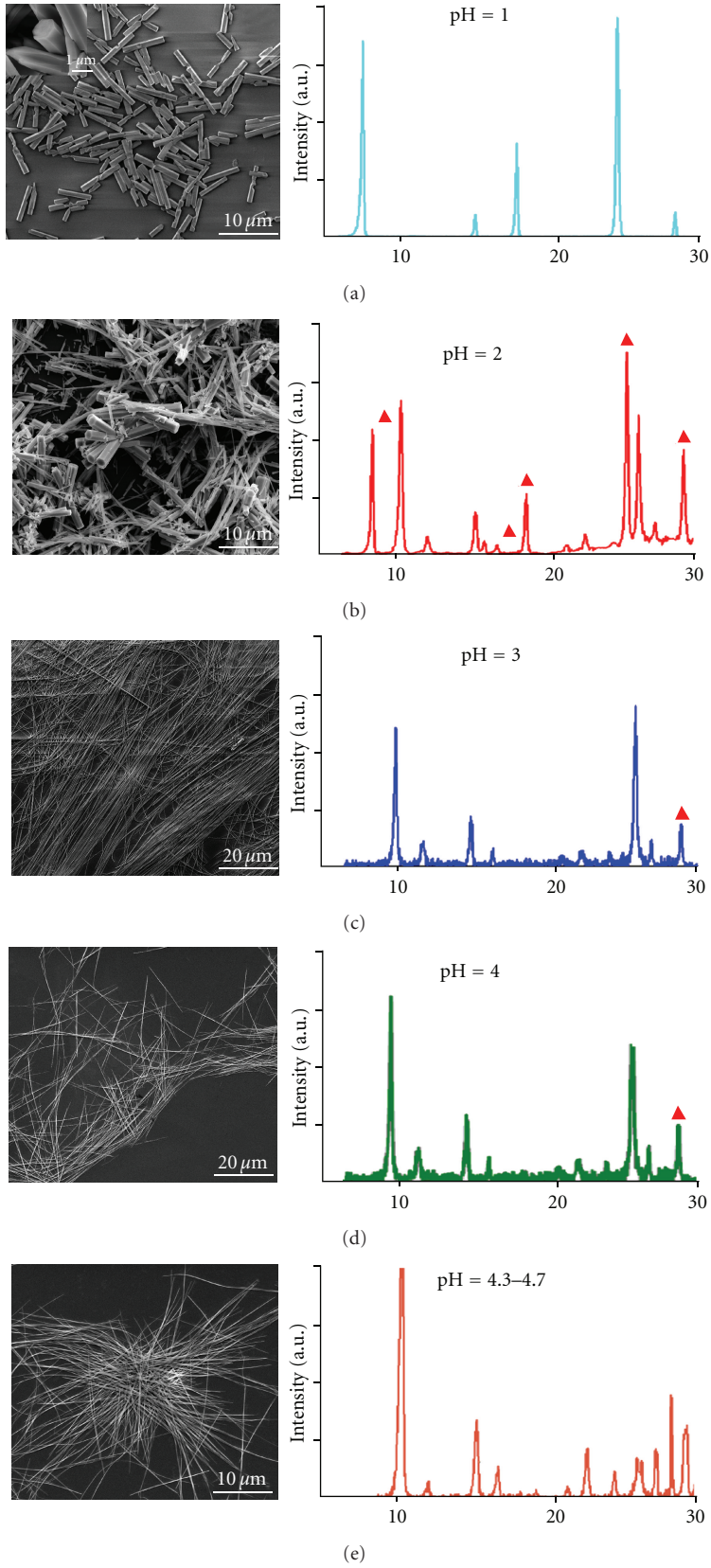

Figure 1: Left panel, shows typical SEM micrographs of 5 kinds of samples synthesized at 30°C under varying pH values of 1.0, 2.0, 3.0, 4.0, and 4.3–4.7, respectively. Right panel is their corresponding XRD spectra. The peaks for $NH_3(MoO_3)_3$ phase are marked by solid red triangles in (b)–(d). Shown in (e), without adding any acid, the mixture solution of $(NH_4)_6Mo_7O_{24}\cdot 4H_2O$ and $AgNO_3$ naturally maintained its pH value in a narrow range of 4.3–4.7 in the whole reaction process.

Their mass ratio in the mixture, ranging from 10 : 1 to 1 : 3, had been systematically studied. The pH value of the starting solutions was controlled with drops of diluted HNO_3 acid. The mixed solution in an open beaker was immersed into a water bath kept at a set temperature between 20 and 80°C, and a magnetic stirrer was used during the whole reaction process. In minutes yellowish-white precipitates were obtained from the mixed solution, and gradually the whole solution turned into porous, paste-like precipitates with some residual water. After centrifuging and rinsing the precipitates with deionized water for 3–6 cycles, the samples were dried in air and characterized by means of scanning electron microscopy (SEM, Tecnai XL30F), X-ray diffraction (XRD, Rigaku D/max-2400) for morphology, transmission electron microscope (TEM, Tecnai G20, 200 kV) for imaging, *in situ* energy-dispersive X-ray (EDX) and selected area electron diffraction (SAED), and Cu spectra for surface binding energy of the Ag atoms. Thermogravimetric analysis (TGA, Q600) was performed in the ambient of pure nitrogen gas.

For the cytotoxicity test, 293E cell line was chosen to be the human cells sample. First, the cells sample was cultured with nutrient medium of DMEM, which contained 10% fetal calf serum to reach a concentration of 60–80% in a culture dish with diameter of 10 cm. Next, the nutrient medium was moved away and the cells were washed out with 2 mL PBS. Then trypsogen was added into the sample for 40 seconds. The pseudo pods of the adherent cells retracted and the cells turned into round shapes. Subsequently, 3 mL nutrient medium of DMEM was added into the sample and the solution was blown with a pipette to suspend cells, meanwhile the number of cells was counted with a count plate. After that, about 3×10^5 cells were taken to each of 12-well plates, and the solution in each well was supplemented to 1 mL with DMEM and stirred until being uniform. At last, the sample was placed at an incubator at 37°C and 5% CO_2, adding in nanowires with certain concentrations. The statement of the cell samples was observed closely after different intervals. For the LB plate antibacterial experiments, the *E. coli* DH5a samples were inverted with PCI-neo-GFP plasmid, and the number of colonies for each trial was counted. The samples were cultured in nutrient Agar (N.A.) at 37°C for 96 hours. For the skin safety experiments, 4 rabbits weighing 2.3–2.5 kg were used. The temperature and humidity of the rabbit hutch were kept at 18–26°C and 40–61%, respectively. Hairs on both sides of the spine of each rabbit were totally sheared away, leaving two pieces of clean skin, each about 3 square centimeters. On one piece of the clean skin, 0.5 mL of 1000 ppm Ag-doped nanowires in deionized water was smeared uniformly, while the other piece was left untreated for contrast.

3. Results and Discussion

The nanowires were synthesized at 30°C from a mixed aqueous solution of $(NH_4)_6Mo_7O_{24}\cdot 4H_2O$ and $AgNO_3$. Various phases of Ag-rich trimolybdate nanomaterials could be obtained in a controlled way when the pH value of the starting solution was adjusted. Figure 1 shows in the left panel 5

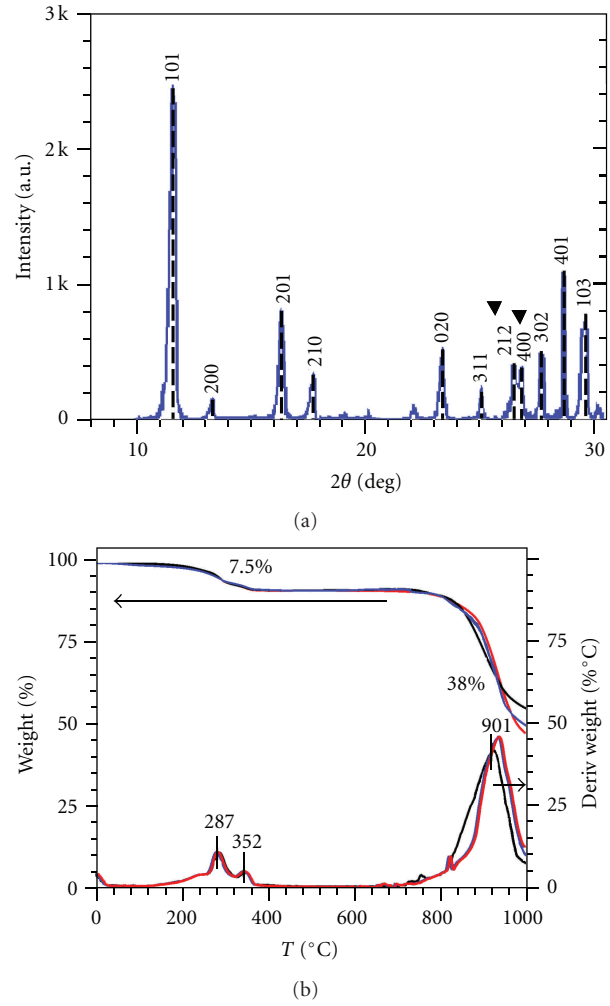

Figure 2: Experimental XRD data (a) and TGA data (b) of $Ag_{2-x}(NH_4)_xMo_3O_{10}\cdot 3H_2O$ nanowires. The two triangles in (a) indicate the peaks having opposite offset direction to that of the rest peaks, as compared to XRD data of $(NH_4)_2Mo_3O_{10}$ (see the Supplementary figure in the Supplementary Material available online at doi: 10.5402/2012/539601).

groups of typical SEM micrographs of our samples made under varying pH values and their corresponding XRD spectra in the right panel. From the XRD spectra we distinguished different crystalline phases in the as-synthesized nanomaterials. When the starting pH value was set at 1.0, hexagonal prisms of the $NH_3(MoO_3)_3$ phase (JCPDS 77-0354) with diameters around one micron were obtained, as shown in Figure 1(a). End product obtained under initial pH of 2.0 consisting of both $NH_3(MoO_3)_3$ (marked by solid red triangles) and $Ag_{2-x}(NH_4)_xMo_3O_{10}\cdot 3H_2O$ phases is shown in Figure 1(b). Nanowires shown in Figure 1(c) and Figure 1(d) were obtained when the initial pH values were set at 3.0 and 4.0, respectively. Their XRD spectra show the major phase of $Ag_{2-x}(NH_4)_xMo_3O_{10}\cdot 3H_2O$ and peaks of the minority $NH_3(MoO_3)_3$ phase (marked by solid red triangles). Here, the chemical formula of $Ag_{2-x}(NH_4)_xMo_3O_{10}\cdot 3H_2O$ was obtained by calculations based on both the experimental

Table 1: Experimental XRD data for $Ag_{2-x}(NH_4)_xMo_3O_{10}\cdot 3H_2O$ nanowires (this work) and $(NH_4)_2Mo_3O_{10}$ (JCPDS 79-1905). The differences in lattice spacings between these two phases, namely d_1 and d_2, are calculated and listed.

hkl	2θ (deg.)	d_1 (Å)	2θ (deg.)	d_2 (Å)	$(d_1 - d_2)$ (Å)	$(d_1 - d_2)/d_2$
101	11.52	7.6748	11.647	7.5915	0.127	1.673%
200	13.2	6.7018	13.423	6.5910	0.223	3.383%
011	15.08	5.8709	15.064	5.8762	0.014	0.238%
201	16.32	5.4273	16.479	5.3748	0.161	2.995%
210	17.70	5.0070	17.809	4.9762	0.110	2.211%
211	20.14	4.4055	20.261	4.3793	0.122	2.786%
301	22.12	4.0152	22.365	3.9718	0.245	6.168%
020	23.34	3.8083	23.434	3.7931	0.095	2.505%
311	25.10	3.5452	25.288	3.519	0.190	5.399%
212	26.28	3.3882	26.235	3.3941	−0.047	−1.385%
400	27.06	3.2925	27.034	3.2955	−0.025	−0.759%
302	27.74	3.2134	27.934	3.1914	0.195	6.110%
401	28.76	3.1018	28.776	3.0998	0.019	0.613%
103	29.58	3.0175	29.621	3.0134	0.041	1.361%

XRD and TGA data that will be discussed in the following sections.

Without adding any acid, the mixture solution of $(NH_4)_6Mo_7O_{24}\cdot 4H_2O$ and $AgNO_3$ naturally maintained its pH value in a narrow range of 4.3–4.7 at 30°C in the whole reaction process. This was attributed to the existence of NH_4^+ ions in the solution [38, 39]. Synthesized under this condition, the end products were uniform and long nanowires, as shown in Figure 1(e).

The blue line in Figure 2(a) plots the XRD spectrum of the nanowires shown in Figure 1(e). It reveals a single crystalline phase that matches well to the tetragonal phase of $(NH_4)_2Mo_3O_{10}$ (JCPDS 79-1905), peaks of which are marked as black lines in Figure 2, with slight offsets. The lattice constants of $(NH_4)_2Mo_3O_{10}$ are $a = 1.3182$ nm, $b = 0.7589$ nm, and $c = 0.9286$ nm. The lattice constants of our tetragonal nanowire phase are calculated to be $a = 1.336$ nm, $b = 0.754$ nm, and $c = 0.921$ nm, where a becomes 1.35% bigger and b and c become 0.65% and 0.82% smaller, respectively. As a result, most lattice spacings of our nanowires are larger than their counterparts of $(NH_4)_2Mo_3O_{10}$ (see Table 1), while the spacings of (212) and (400) are smaller, marked by black triangles in Figure 2(a). Also, the XRD spectrum of our samples matches well to that of $NaNH_4Mo_3O_{10}\cdot H_2O$ (JCPDS 36-0335, not shown here), and again with slight offsets, indicating the similarity among these three kinds of tetragonal lattices. This is the first evidence that in our nanowires Ag atoms have taken the lattice positions.

The TGA data of the samples also reveal that Ag atoms substitute the $(NH_4)^+$ sites in the crystalline lattices. Figure 2(b) shows TGA data of three different batches of the nanowires synthesized under the same conditions shown in Figure 1(e). The three measurement curves match well to each other. The first step of loss in weight, about 7.5%, was measured at around 280–370°C, corresponding to the weight percentage of NH_3 and H_2O released from the nanowires. The second peak of loss in weight, about 38%, was measured at around 800–1000°C, corresponding to the weight percentage of released Ag_2O. Calculated from the TGA data, comparing the similarity of its XRD spectrum to those of $NaNH_4Mo_3O_{10}\cdot H_2O$ and $(NH_4)_2Mo_3O_{10}$, we determined the chemical formula of the nanowires to be $Ag_{2-x}(NH_4)_xMo_3O_{10}\cdot 3H_2O$, where $x \leq 0.5$.

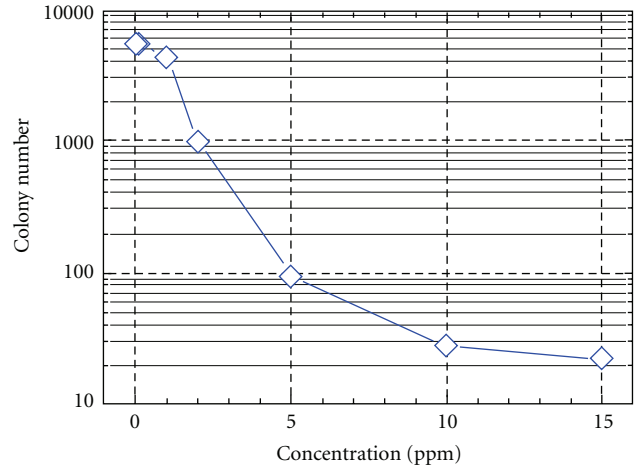

Figure 3: Results of LB plate culture experiment of the $Ag_{2-x}(NH_4)_xMo_3O_{10}\cdot 3H_2O$ nanowires against *E. coli* DH5a. It shows that 2 ppm is the critical concentration for antibacteria. When the concentration increases to 5 ppm, the number of colonies decreases to 2% of that without nanowires.

When the Ag-doped trimolybdate nanowires were used in a high concentration, they could efficiently eliminate the growth of bacteria. Figure 3 shows the results of a culture experiment using Lysogeny broth (LB) plate, a more quantitative test for the antibacterial ability of the $Ag_{2-x}(NH_4)_xMo_3O_{10}\cdot 3H_2O$ against *E. coli* DH5a. It shows that 2 ppm of nanowires in the sample is the critical value of antibacteria. When the concentration increased to 5 ppm, the number of colonies decreased to 2% of that without

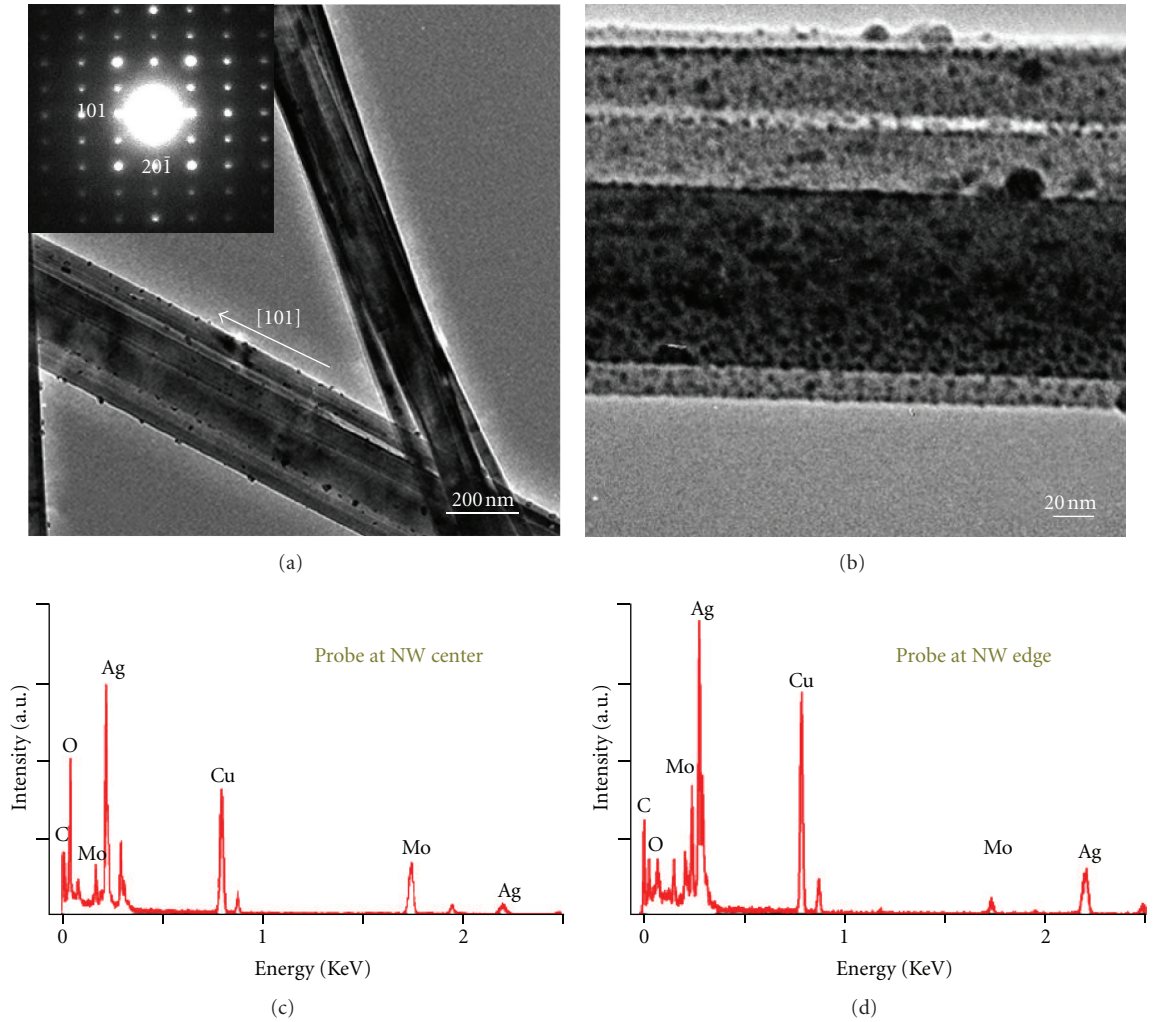

FIGURE 4: (a) A low magnification TEM image of $Ag_{2-x}(NH_4)_xMo_3O_{10}\cdot 3H_2O$ nanowires. The inset is a typical SAED of a single nanowire, showing single crystalline phase and the growth direction [101] of each nanowire. (b) A close look at a nanowire revealing a large amount of nanoparticles. (c) and (d) EDX spectra of the center region and the edge region of the same nanowire, respectively.

nanowires. That is, as much as 98% of the bacteria are inhibited.

We have tested the cytotoxicity of the as-synthesized nanowires to find out the concentration range in which the nanowires are safe to human cells and at the same time have an effective antimicrobial effect [40]. Here, 293E cell line was chosen to be the human cells sample. The results are shown in Figure 6. The blue (dark and light) regions show the concentration range in which nanowires are friendly to human cells but cannot inhibit the growth of microbes effectively. In the red (dark and light) regions the nanowires are antimicrobial but also do harm human cells. The green region is the concentration window in which the nanowires are both friendly to human cells and have an effective antimicrobial effect. The results show that the safety window of concentration depends much on the reaction time duration. Within 4 hours, the ratio of the highest to the lowest concentrations in the safe region is 100, and this ratio decreases to 15 at 24 hours and 2 at 96 hours.

Two major elements in the $Ag_{2-x}(NH_4)_xMo_3O_{10}\cdot 3H_2O$ nanowires are expected to have the antibacterial nature, that is, the Ag^+ ions and the Mo^{6+} ions of the composite, both of which have been reported previously [1–16, 41–43]. In this work, we have also observed a large amount of Ag-rich nanoparticles on surface of the nanowires. These Ag-rich nanoparticles may also contribute greatly to the observed antibacterial nature.

Morphology imaging and SAED analyses of the as-synthesized $Ag_{2-x}(NH_4)_xMo_3O_{10}\cdot 3H_2O$ nanowires with a TEM showed that the nanowires had a single crystalline structure with a growth direction [101] (inset of Figure 4). On the surface of the nanowires, a large amount of randomly distributed dark nanoparticles were observed. The *in situ* EDX spectra of individual nanowires revealed that, when the electron-beam probe was moved from the center to the edge of the same nanowire, the relative atomic ratio of Ag over Mo was remarkably increased, as typically shown in Figures 4(c) and 4(d), respectively. This suggests that the dark

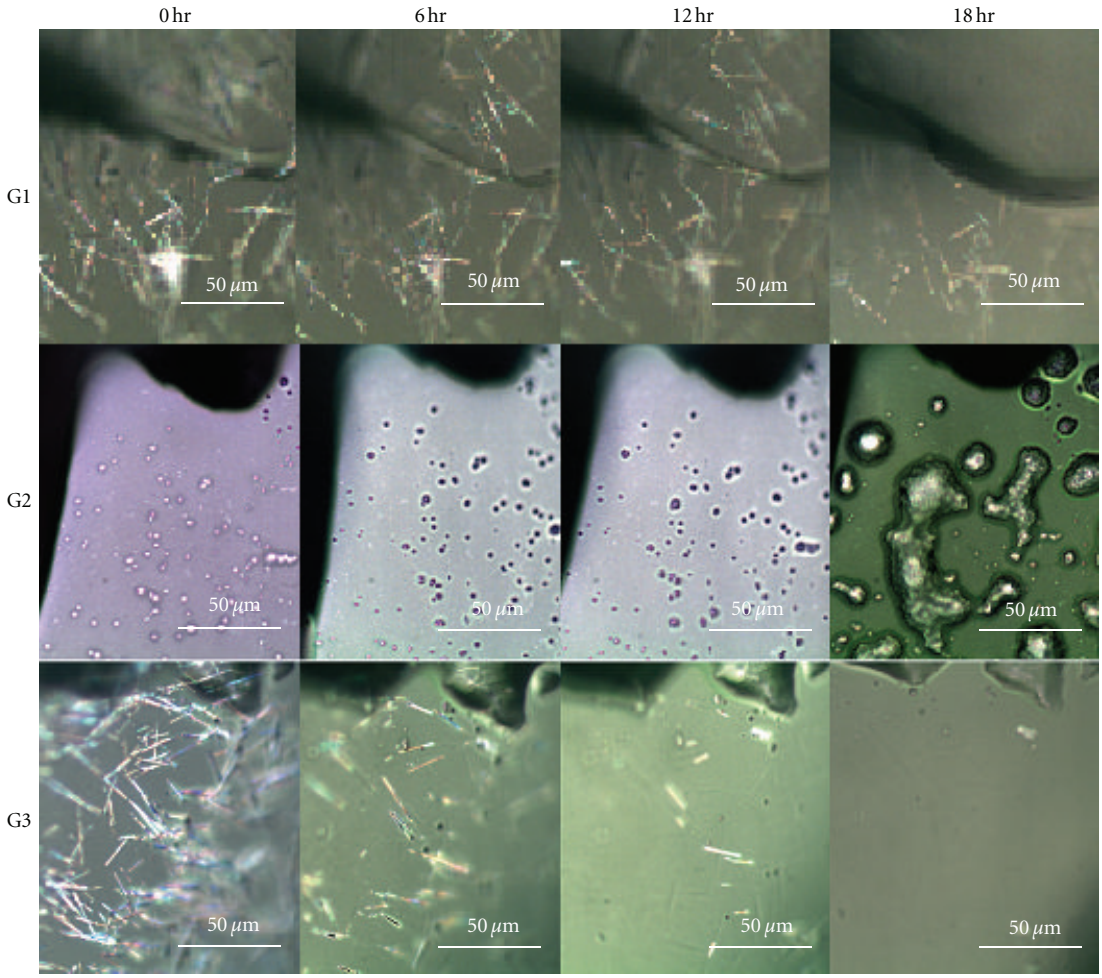

Figure 5: Optical images of 3 samples that were spread on the same kind of N.A. base and cultured under the same conditions at 40°C for 18 hours. G1: pure *Staphylococcus aureus* bacteria. G2: *Staphylococcus aureus* bacteria mixed with dry $Ag_{2-x}(NH_4)_xMo_3O_{10}\cdot 3H_2O$ nanowires. G3: pure $Ag_{2-x}(NH_4)_xMo_3O_{10}\cdot 3H_2O$ nanowires. *Staphylococcus aureus* bacteria had been sufficiently eliminated with the presence of the nanowires. In G2, the nanowires originally seen on the N.A. surface disappeared gradually after 6–18 hours. In G3, the nanowires kept their original shapes.

nanoparticles on the nanowires are Ag rich, most probably Ag_2O particles, which are formed in the synthesis process. Under the irradiation of an intense electron beam, the dark particles could move slightly on the nanowire surface. The XPS spectra of the nanowires consisted of peaks for Mo, Ag, O, and N. The binding energy of Ag 3d was measured to be 367.97 eV, indicating that Ag atoms occurred in the form of Ag_2O. The peak for Mo 3d was measured to be 232.75 eV, showing its chemical status of α-MoO_3 (232.6 eV). The atomic ratio of Ag to Mo, indicated by the XPS data, was about 9 : 16.

We also performed experiments to filter the natural water taken from the *Weiming Lake* on the campus of Peking University with nanowire-treated filtering paper. Each layer of the nanowire-treated filtering paper was dipped in a solution of the $Ag_{2-x}(NH_4)_xMo_3O_{10}\cdot 3H_2O$ nanowires and dried in air. Repeated experiments showed that, when the natural water was filtered through 4–6 layers of the nanowire-treated filtering paper, 95–99% of the natural microbes in the lake water, although unknown, were eliminated (see the Supplementary figure).

We note that both nanowires of pure $(NH_4)_2Mo_3O_{10}$ and $NaNH_4Mo_3O_{10}\cdot H_2O$ phases are easily dissolvable in deionized water [39], while the nanowires shown in Figures 1(c), 1(d), and 1(e) are not. However, they can be dissolved in mild acidic solutions. As shown in Figure 5, we have observed clear evidence that these nanowires could be dissolved by the chemicals released from the bacteria during their metabolism processes. Group 1 (G1) images show *Staphylococcus aureus* bacteria cultured on a base of N.A. at 40°C for 18 hours. Group 2 (G2) images show *Staphylococcus aureus* bacteria mixed with dry $Ag_{2-x}(NH_4)_xMo_3O_{10}\cdot 3H_2O$ nanowires cultured on the same N.A. base at 40°C for 18 hours. For comparison, Group 3 (G3) images show pure $Ag_{2-x}(NH_4)_xMo_3O_{10}\cdot 3H_2O$ nanowires on N.A. experimented under the same condition. The *Staphylococcus aureus* bacteria have been sufficiently eliminated with the presence of the nanowires. We note that, in G2, the nanowires originally seen on the N.A. surface disappeared gradually

Time (hr) \ C (ppm)	0	0.5	1	2	5	7.5	10	15	20	50	100
4	B. I.	B. I.	n	n	n	n	n	n	n	n	n
12	B. I.	B. I.	n	n	n	n	n	n	n	L. F.^{s}	L. F.
24	B. I.	B. I.	n	n	n	n	n	n	L. F.^{s}	L. F.	C. S.
48	B. I.	B. I.	B. I.^{s}	n	n	n	n	n	L. F.	C. S.	A.
96	B. I.	B. I.	B. I.^{s}	B. I.^{s}	n	n	n	L. F.^{s}	C. S.	A.	A.

Figure 6: Results of the cytotoxicity test for $Ag_{2-x}(NH_4)_xMo_3O_{10}\cdot 3H_2O$ nanowires in 293E human cells. The experiments were performed under varying concentrations (C) in unit of part per million (ppm) of the nanowires used and varying reaction times with the cells (in hours). B.I.: Bacterial infection; n.: normal; L.F.: loss form; C.S.: contents spill; A.: apoptosis; and s: slightly. In the blue (dark and light) regions the nanowires are friendly to human cells but show no obvious antimicrobial effect. In the green (normal) region the nanowires are both friendly to human cells and have an effective antimicrobial effect. In the red (dark and light) regions the nanowires have an effective antimicrobial effect but also attack human cells.

after 6–18 hours, while, in G3, the nanowires kept their original shapes. This nature should be favorable for certain biological applications, for example, once these nanowire carriers have accomplished their missions, they themselves might be naturally dissolved in the cell or tissue and be removed out of the target regions.

Because the Ag-rich nanoparticles are dispersed on the $Ag_{2-x}(NH_4)_xMo_3O_{10}\cdot 3H_2O$ nanowires, while the nanowires should be able to wrap on fibers easily, this material may be applied in fabrication of antimicrobial yarns and clothes. We have performed a skin sensitivity test of the nanowires on rabbits for fourteen days. The concentration used in the experiments was 1000 ppm, much higher than the actual concentration that may apply. The skin of rabbit stays in good condition free of erythema or dropsy in the period of experiment, proving the safety of skin with this kind of nanowires.

4. Conclusion

We have presented a novel single crystalline trimolybdate nanowire that carries a large amount of Ag ions in its lattice and Ag-rich nanoparticles on its surface. These nanowires kill *E. coli*, *Staphylococcus aureus*, and some unknown microbes in raw natural water with high efficiency. They are not dissolvable in deionized water but could be dissolved in mild acidic solutions or by metabolic chemicals released from bacteria; therefore they may have a great potential for biological applications. For instance, if such nanowires are applied as drug carrier, they could be naturally dissolved and removed out of the target regions after the mission is completed.

Acknowledgments

The authors are grateful to the National Science Foundation of China (Grant no. 11074010 and no. 60925003) and MOST of China (Grant no. 2011CB933002) for financial support. They thank Professor Yuxin Yin for valuable discussions.

References

[1] H. S. Rosenkranz and H. S. Carr, "Silver sulfadiazine: effect on the growth and metabolism of bacteria," *Antimicrobial Agents and Chemotherapy*, vol. 2, no. 5, pp. 367–372, 1972.

[2] P. D. Bragg and D. J. Rainnie, "The effect of silver ions on the respiratory chain of Escherichia coli," *Canadian Journal of Microbiology*, vol. 20, no. 6, pp. 883–889, 1974.

[3] W. J. A. Schreurs and H. Rosenberg, "Effect of silver ions on transport and retention of phosphate by Escherichia coli," *Journal of Bacteriology*, vol. 152, no. 1, pp. 7–13, 1982.

[4] C. Haefeli, C. Franklin, and K. Hardy, "Plasmid-determined silver resistance in pseudomonas stuzeri isolated from a silver mine," *Journal of Bacteriology*, vol. 158, no. 1, pp. 389–392, 1984.

[5] J. J. Castellano, S. M. Shafii, F. Ko et al., "Comparative evaluation of silver-containing antimicrobial dressings and drugs," *International Wound Journal*, vol. 4, no. 2, pp. 114–140, 2007.

[6] H. J. Klasen, "Historical review of the use of silver in the treatment of burns," *Burns*, vol. 27, no. 3, pp. 301–302, 2001.

[7] D. M. Eby, N. M. Schaeublin, K. E. Farrington, S. M. Hussain, and G. R. Johnson, "Lysozyme catalyzes the formation of antimicrobial silver nanoparticles," *ACS Nano*, vol. 3, no. 4, pp. 984–994, 2009.

[8] D. T. Schoen, A. P. Schoen, L. Hu, H. S. Kim, S. C. Heilshorn, and Y. Cui, "High speed water sterilization using one-dimensional nanostructures," *Nano Letters*, vol. 10, no. 9, pp. 3628–3632, 2010.

[9] M. Rai, A. Yadav, and A. Gade, "Silver nanoparticles as a new generation of antimicrobials," *Journal of Biotechnology Advances*, vol. 27, no. 1, pp. 76–83, 2009.

[10] J. R. Morones, J. L. Elechiguerra, A. Camacho et al., "The bactericidal effect of silver nanoparticles," *Nanotechnology*, vol. 16, no. 10, Article ID 101088, pp. 2346–2353, 2005.

[11] J. L. Elechiguerra, J. L. Burt, J. R. Morones et al., "Interaction of silver nanoparticles with HIV-I," *Journal of Nanobiotechnology*, vol. 3, no. 6, Article ID 101186, 2005.

[12] R. W. Sun, R. Chen, N. P. Chung, C. Ho, C. S. Lin, and C. Che, "Silver nanoparticles fabricated in hepes buffer exhibit cytoprotective activities toward HIV-I infected cells," *Chemical Communications*, no. 40, pp. 5059–5061, 2005.

[13] L. Lu, R. W. Sun, R. Chen et al., "Silver nanoparticles inhibit hepatitis B virus replication," *Antiviral Therapy*, vol. 13, no. 2, pp. 252–262, 2008.

[14] H. H. Lara, N. V. Ayala-Nuñez, L. Ixtepan-Turrent, and C. Rodriguez-Padilla, "Mode of antiviral action of silver nanoparticles against HIV-1," *Journal of Nanobiotechnology*, vol. 8, no. 1, Article ID 20145735, 2010.

[15] J. L. Speshock, R. C. Murdock, L. K. Braydich-Stolle, A. M. Schrand, and S. M. Hussain, "Interaction of silver nanoparticles with Tacaribe virus," *Journal of Nanobiotechnology*, vol. 8, no. 19, Article ID 101186, 2010.

[16] O. C. Farokhzad and R. Langer, "Impact of nanotechnology on drug delivery," *ACS Nano*, vol. 3, no. 1, pp. 16–20, 2009.

[17] J. S. Kim, E. Y. Kuk, K. N. Yu et al., "Antimicrobial effects of silver nanoparticles," *Nanomedicine: Nanotechnology, Biology, and Medicine*, vol. 3, no. 1, pp. 95–101, 2007.

[18] C. R. Martin and P. Kohli, "The emerging field of nanotube biotechnology," *Nature Reviews Drug Discovery*, vol. 2, no. 1, pp. 29–37, 2003.

[19] C. Z. Li, Y. Liu, and J. H. T. Luong, "Impedance sensing of DNA binding drugs using gold substrates modified with gold nanoparticles," *Analytical Chemistry*, vol. 77, no. 2, pp. 478–485, 2005.

[20] A. Bianco, K. Kostarelos, and M. Prato, "Applications of carbon nanotubes in drug delivery," *Current Opinion in Chemical Biology*, vol. 9, no. 6, pp. 674–679, 2005.

[21] Z. Liu, K. Chen, C. Davis et al., "Drug delivery with carbon nanotubes for *in vivo* cancer treatment," *Cancer Research*, vol. 68, no. 16, pp. 6652–6660, 2008.

[22] A. A. Bhirde, V. Patel, J. Gavard et al., "Targeted killing of cancer cells *in vivo* and *in vitro* with EGF-directed carbon nanotube-based drug delivery," *ACS Nano*, vol. 3, no. 2, pp. 307–316, 2009.

[23] L. Zhang, J. M. Chan, F. X. Gu et al., "Self-assembled lipid-polymer hybrid nanoparticles: a robust drug delivery platform," *ACS Nano*, vol. 2, no. 8, pp. 1696–1702, 2008.

[24] Y. Chen, H. Chen, D. Zeng et al., "Core/shell structured hollow mesoporous nanocapsules: a potential platform for simultaneous cell imaging and anticancer drug delivery," *ACS Nano*, vol. 4, no. 10, pp. 6001–6013, 2010.

[25] D. Baram-Pinto, S. Shukla, N. Perkas, A. Gedanken, and R. Sarid, "Inhibition of herpes simplex virus type 1 infection by silver nanoparticles capped with mercaptoethane sulfonate," *Bioconjugate Chemistry*, vol. 20, no. 8, pp. 1497–1502, 2009.

[26] M. Liong, J. Lu, M. Kovochich et al., "Multifunctional inorganic nanoparticles for imaging, targeting, and drug delivery," *ACS Nano*, vol. 2, no. 5, pp. 889–896, 2008.

[27] D. He, B. Hu, Q. F. Yao, K. Wang, and S. H. Yu, "Large-scale synthesis of flexible free-standing SERS substrates with high sensitivity: electrospun PVA nanofibers embedded with controlled alignment of silver nanoparticles," *ACS Nano*, vol. 3, no. 12, pp. 3993–4002, 2009.

[28] F. Liu, Z. Cao, C. Tang, L. Chen, and Z. Wang, "Ultrathin diamond-like carbon film coated silver nanoparticles-based substrates for surface-enhanced raman spectroscopy," *ACS Nano*, vol. 4, no. 5, pp. 2643–2648, 2010.

[29] L. Lacerda, A. Bianco, M. Prato, and K. Kostarelos, "Carbon nanotubes as nanomedicines: from toxicology to pharmacology," *Advanced Drug Delivery Reviews*, vol. 58, no. 14, pp. 1460–1470, 2006.

[30] D. B. Warheit, B. R. Laurence, K. L. Reed, D. H. Roach, G. A. M. Reynolds, and T. R. Webb, "Comparative pulmonary toxicity assessment of single-wall carbon nanotubes in rats," *Toxicological Sciences*, vol. 77, no. 1, pp. 117–125, 2004.

[31] A. Magrez, S. Kasas, V. Salicio et al., "Cellular toxicity of carbon-based nanomaterials," *Nano Letters*, vol. 6, no. 6, pp. 1121–1125, 2006.

[32] C. W. Lam, J. T. James, R. McCluskey, and R. L. Hunter, "Pulmonary toxicity of single-wall carbon nanotubes in mice 7 and 90 days after intractracheal instillation," *Toxicological Sciences*, vol. 77, no. 1, pp. 126–134, 2004.

[33] L. Wang, S. Luanpitpong, V. Castranova et al., "Carbon nanotubes induce malignant transformation and tumorigenesis of human lung epithelial cells," *Nano Letters*, vol. 11, no. 7, Article ID 101021, pp. 2796–2803, 2011.

[34] L. Cheng, Q. Shao, M. Shao, X. Wei, and Z. Wu, "Photoswitches of one-dimensional Ag_2MO_4(M=Cr, Mo, and W),"" *Journal of Physical Chemistry C*, vol. 113, no. 5, pp. 1764–1768, 2009.

[35] W. Zhang and S. T. Oyama, "In situ laser Raman studies of intermediates in the catalytic oxidation of ethanol over supported molybdenum oxide," *Journal of Physical Chemistry*, vol. 100, no. 25, pp. 10759–10767, 1996.

[36] X. Cui, S. H. Yu, L. Li et al., "Selective synthesis and characterization of single-crystal silver molybdate/tungstate nanowires by a hydrothermal process," *Chemistry*, vol. 10, no. 1, pp. 218–223, 2004.

[37] W. Lasocha, J. Jansen, and H. Schenk, "Application of a new method for the determination of accurate intensities from powder diffraction data. crystal structure determination of fibrillar silver trimolybdate," *Journal of Solid State Chemistry*, vol. 109, no. 1, pp. 1–4, 1994.

[38] W. W. Gong, J. W. Xue, K. Zhang et al., "Room temperature synthesis of $K_2Mo_3O_{10} \cdot 3H_2O$ nanowires in minutes," *Nanotechnology*, vol. 20, no. 21, Article ID 215603, 2009.

[39] W. W. Gong, J. W. Xue, Q. W. Zhuang, X. D. Wu, and S. Y. Xu, "Fabrication of nanochannels with water-dissolvable nanowires," *Nanotechnology*, vol. 21, no. 19, Article ID 195302, 2010.

[40] P. V. AshaRani, G. L. K. Mun, M. P. Hande, and S. Valiyaveettil, "Cytotoxicity and genotoxicity of silver nanoparticles in human cells," *ACS Nano*, vol. 3, no. 2, pp. 279–290, 2009.

[41] B. Hasenknopf, "Polyoxometalates: introduction to a class of inorganic compounds and their biomedical applications," *Frontiers in Bioscience*, vol. 10, no. 1, pp. 275–287, 2005.

[42] A. Ogata, S. Mitsui, H. Yanagie et al., "A novel anti-tumor agent, polyoxomolybdate induces apoptotic cell death in AsPC-1 human pancreatic cancer cells," *Biomedicine and Pharmacotherapy*, vol. 59, no. 5, pp. 240–244, 2005.

[43] A. Ogata, H. Yanagie, E. Ishikawa et al., "Antitumour effect of polyoxomolybdates: induction of apoptotic cell death and autophagy in *in vitro* and *in vivo* models," *British Journal of Cancer*, vol. 98, no. 2, pp. 399–409, 2008.